Plasma-wall interaction and Hall thruster microturbulence

IEPC-2015-339／ISTS-2015-b-339

Presented at Joint Conference of 30th International Symposium on Space Technology and Science, 34th International Electric Propulsion Conference and 6th Nano-satellite Symposium
Hyogo-Kobe, Japan
July 4–10, 2015

Sedina Tsikata *
ICARE, Electric Propulsion Team, UPR 3021 CNRS, Orléans, France

Cyrille Honoré†
LPP, Ecole Polytechnique, UMR 7648 CNRS, Palaiseau, France

Anne Héron‡
CPHT, Ecole Polytechnique, UMR 7644 CNRS, Palaiseau, France

Aude Pétin§ and Stéphane Mazouffre¶
ICARE, Electric Propulsion Team, UPR 3021 CNRS, Orléans, France

Plasma instabilities strongly influence the nature of the plasma-wall interaction, and consequently, features such as the electron current in devices such as Hall thrusters. The electron cyclotron drift instability, implicated in anomalous electron transport and identified in both simulations and coherent Thomson scattering experiments, plays a subtle role in such interaction, via non-linear coupling to the electron emission. In this paper, the mode features in the presence of standard $BNSiO_2$ walls and low-emission carbon inserts are determined via coherent scattering. These results are situated in the context of recent findings from radial-azimuthal particle-in-cell simulations. Modifications to thruster discharge current features due to the use of carbon velvet are also described. The use of a non-emissive material results in major changes to the electric field profile, microturbulence characteristics and discharge features.

Nomenclature

k	= mode wavenumber
$S(k,\omega), S(k)$	= dynamic form factor, static form factor
SEE	= secondary electron emission
ϵ^*	= electron crossover energy
Id, Ud	= discharge current, voltage
ω_p	= plasma frequency

*Research Scientist, Electric Propulsion Team, ICARE, sedina.tsikata@cnrs-orleans.fr
†Research Engineer, Laboratoire de Physique des Plasmas, cyrille.honore@polytechnique.edu
‡Research Scientist, Centre de Physique Théorique, anne.heron@polytechnique.edu
§PhD student, Electric Propulsion Team, ICARE, aude.petin@cnrs-orleans.fr
¶Research Scientist, Electric Propulsion Team, ICARE, stephane.mazouffre@cnrs-orleans.fr

I. Introduction

The complexity of plasma-wall interaction poses a challenge for modelling efforts of the Hall thruster discharge. In particular, a lack of clear knowledge concerning sheath dynamics, particle energies near the walls, and the role played by secondary electron emission means that predictive simulations for the discharge are still beyond reach.

The picture is further complicated by plasma instabilities. The electron cyclotron drift instability[1,2] was first identified by Adam et al.[3] in axial-azimuthal particle-in-cell (PIC) simulations as a major contributor to the anomalous electron mobility observed at the thruster exit. The instability was later identified experimentally using a specially-devised coherent (or collective) Thomson scattering (CTS) diagnostic.[4] The experimental and simulation results have been accompanied with linear kinetic theory modelling, and a high level of detail is now available regarding the mode features and behavior.

Our understanding of the mode behavior has been further broadened by the inclusion of wall effects in recent radial-azimuthal simulations.[5] These simulations demonstrate that the mode's contribution to the electron current takes two forms: its "direct" contribution via interaction with the electrons undergoing the azimuthal drift, and an "indirect" contribution from its heating of the plasma which results in increased wall emission.

This work focuses on recent attempts to better understand the nature of this coupling. We contrast thruster operation and microturbulence features with two materials: standard $BNSiO_2$ and low-emissivity carbon velvet material, and attempt to understand the origin of the observered differences. We also situate experimental work in the context of recent results from numerical simulations. These analyses are performed using CTS measurements of the mode amplitude, qualitative electric field measurements using an emissive probe, and radial-azimuthal PIC simulation results.

II. Experimental details and simulations

A. Coherent Thomson scattering experiments

In the coherent Thomson scattering regime, the correlated movements of electrons are observed, rather than their individual thermal fluctuations. Such observations are possible at scales on the order of and exceeding the electron Debye length, and such correlations can be induced by the presence of a wave. The scattered electric field amplitude is proportional to the spatial Fourier transform of the electron density, and provided observation length scales are set to the same scale as the spatial correlation in the electron positions, the coherent scattered signal can be detected. This can permit identification and characterization of a wave at these scales.

The PRAXIS (PRopulsion Analysis eXperiments via Infrared Scattering) coherent Thomson diagnostic makes use of the principles outlined above. Full details on the diagnostic are provided elsewhere;[6] it uses a 40 W CO_2 laser for scattering and has been specifically designed for the identification of the electron cyclotron instability initially identified in simulations.[3] The diagnostic has been designed for very high sensitivity, permitting the measurement of electron density fluctuations of rates below 1% with respect to the mean plasma density. The resonance condition for the excitation of the instability,

$$k_y V_d = n\omega_{ce} \tag{1}$$

where k_y is the azimuthal wavenumber, V_d the electron drift velocity, n an integer one or greater, and ω_{ce} the electron cyclotron angular frequency, means that expected length scales are on the order of a millimeter and below. The PRAXIS diagnostic allows for fluctuations of the electron density to be measured at these scales (between 0.4 and 2 mm in the current design), even in plasma regions characterized by high electron temperatures and magnetic fields. Such measurements are impossible via any other conventional means.

To permit comparisons to existing data, measurements were carried out using the 1.5 kW PPS-1350ML® thruster. This thruster is a laboratory model of the Snecma PPS-1350® model and is similar in most respects to the well-known SPT-100. For the experiments discussed in this paper, the thruster is typically operated at varying voltages at a flow rate of 3.5 mg/s and coil current of 4.3 A.

Carbon velvet is an engineered material, supplied by Energy Science Laboratories Inc. (USA), consisting of vertical carbon fibers on a graphite substrate. The choice of this material for study was motivated by intriguing results obtained by Dr. Y. Raitses (PPPL), who was the first to use it as a wall material for

Hall thruster studies. The material's property of near-zero emissivity is guaranteed by its particle-trapping fibers. Raitses and colleagues found[7,8] that the use of carbon velvet electrodes resulted in a saturation of the thruster discharge current at high voltages, a reduction in plume angle, and an increase in electron temperature attained at high voltages - all indicative of improved thruster performance. In this work, we examine modifications to thruster behavior with a focus on how microturbulence is modified by the use of such a material. In carbon velvet experiments, the carbon velvet inserts replace the last 8 mm of the inner and outer channels near the thruster exit (Fig. 1(a)), allowing coverage of the known ionization region for the thruster. The inserts are designed such that the fibers remain flush with the rest of the chamber walls (which are of $BNSiO_2$). The inserts used have carbon fibers of 20 μm diameter and 1 mm height.

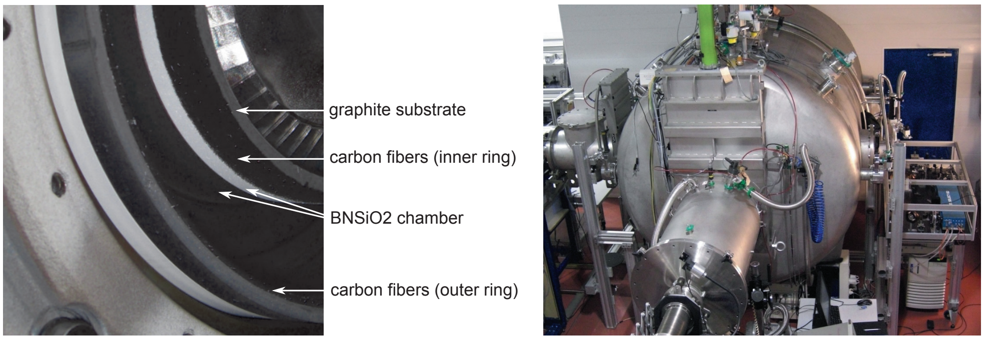

(a) (b)

Figure 1. (a) Photo of carbon velvet rings mounted on the 1.5 kW PPS-1350ML® thruster, (b) photo of the PRAXIS optical bench setup (to the right of the vacuum vessel) at the PIVOINE national thruster facility

B. Emissive probe measurements

Emissive probe measurements were performed in later experiments using an emissive probe attached to a fast-displacement piezoelectric translation stage; in experiments the axial range covered is [-25, 15] mm with respect to an exit plane reference position of 0 mm. The plasma potential measurements made using the probe are derived to provide the electric field profiles. The probe measurements did suffer from some reproducibility problems related to insulation from the plasma, but provided a qualitative idea of the general tendency of the electric field to evolve with voltage. These qualitative measurements were necessary for interpretations of the collective scattering data. Further details on the probe design may be found elsewhere.[9] Measurements in this study concern only axial displacements with the probe aligned with the center of thruster channel.

C. PIC simulations

Explicit particle-in-cell simulations by Héron and Adam have focused most recently on studying radial effects.[5] In this paper, we will discuss some of the simulation results in a radial-azimuthal geometry in the context of our experiments on the electron cyclotron instability. Further details are provided in their published work, but we note a few important details concerning the simulations.

The radial magnetic field B_r imposed in simulations satisfies the condition $rB_r = constant$, where r is the radius. With the axial coordinate absent from the simulations, an axial electric field must be imposed. In contrast to self-consistent azimuthal-axial simulations,[3] the electric field does not change to reflect variations in conductivity. As we will see, this may account for some differences between experiments and simulations. A uniform electric field is imposed, resulting in a faster electron drift velocity at the outer wall than at the inner wall, and solid rotation of the plasma. Collisions and ionization are largely neglected in the vicinity of the thruster exit plane, where these simulations are relevant.

The simulations use the secondary electron emission model described by Barral and colleagues,[11] where the secondary electron emission rate $\sigma(\epsilon_p)$ is given by

$$\sigma(\epsilon_p) = \sigma(0) + \frac{\epsilon_p}{\epsilon^*}(1 - \sigma(0)) \tag{2}$$

where ϵ_p is the electron energy, and $\sigma(0)$ and ϵ^* are the attachment probability and crossover energy respectively, both material-dependent. $\sigma(0)$ is a constant equal to the sum of the elastic and inelastic reflection rates.

Simulation results discussed here concern the SPT-100 thruster (and are applicable to the PPS-1350ML®). The electric field maximum value is 1 - 3 $\times$ 10^4 V/m, and B is 150 G. The mean electron density is 3 $\times$ 10^{17} m^{-3}. For $BNSiO_2$, ϵ^* is 50 eV and $\sigma(0)$ set to 0.5.

III. Discharge current features

We start by examining the general discharge current characteristics. The discharge current amplitudes as a function of voltage differ for $BNSiO_2$ and carbon velvet, as shown in Fig. 2(a) (an anode flow rate of 3.5 mg/s). For $BNSiO_2$, the mean discharge current remains flat from 100 to 500 V. With carbon velvet, the mean discharge current starts to rise after 200 V, and the mean values are consistently higher than those encountered with $BNSiO_2$.

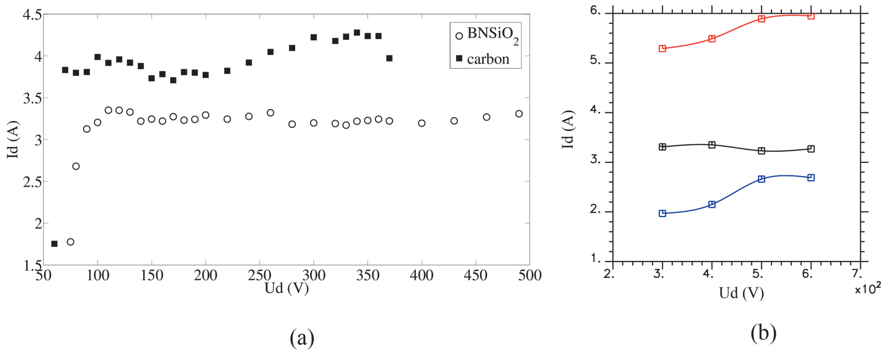

Figure 2. (a) Mean discharge current Id as a function of discharge voltage Ud for $BNSiO_2$ and carbon velvet, (b) axial-azimuthal simulation of discharge current variation with discharge voltage; in black, ion current; in blue, electron current; in red, total current. In simulations, an increase in the electron current is evident even in the absence of radial contributions such as wall emission.

The observation of higher mean currents with carbon velvet appears to be a counterintuitive result for a non-emissive material. However, changing the material emissivity in the acceleration region produces effects which are more subtle than a mere change in the number of electrons emitted from the walls. To understand this, we consider a PIC simulation result which entirely neglects the radial dimension (the original axial-azimuthal simulations[3]). The mean current as a function of discharge voltage is shown in Fig. 2(b). The ion current (black) is unvarying over the 300 V range shown. However, the electron current (blue) increases with voltage, resulting in an overall increase in the mean current, which occurs in the absence of any consideration of a wall contribution.

This leads us to conclude that the high mean currents observed with carbon velvet, due to increased electron current, may be fed by a source other than pure wall emission. The source of this additional current could be the electron cyclotron instability; this will be discussed in further detail shortly.

The discharge current standard deviation (σId) evolves differently for the two materials, as Fig. 3 shows. As seen in Fig. 3(a), both $BNSiO_2$ and velvet show strong oscillations at voltages below 150 V. However, different regimes emerge for the two materials as the voltage increases, with carbon velvet oscillations pronounced between 300 and 350 V. At 300 V, the $BNSiO_2$ discharge current shows a peak at around 55 kHz, while an intense, lower-frequency peak at 20 kHz is observed with carbon velvet at the same voltage (Fig. 3(b)). Apart from the existence of marked discharge current fluctuations at high voltages, the discharge was also observed to be less stable with carbon velvet. At voltages exceeding 400 V, the discharge was difficult to maintain and intermittent current peaks of up to 50 A were observed.

At this juncture, it is worth comparing these observations with those made by Raitses and colleagues for boron nitride and carbon velvet walls. In our study, the discharge current profile remains relatively flat for both materials as discharge voltage increases, which is expected in standard operation. Raitses and colleagues observed both a linear increase in discharge current with discharge voltage in a transitional regime[7] for BN, and flatter current profiles in steady state operation for both materials. They observed lower mean currents

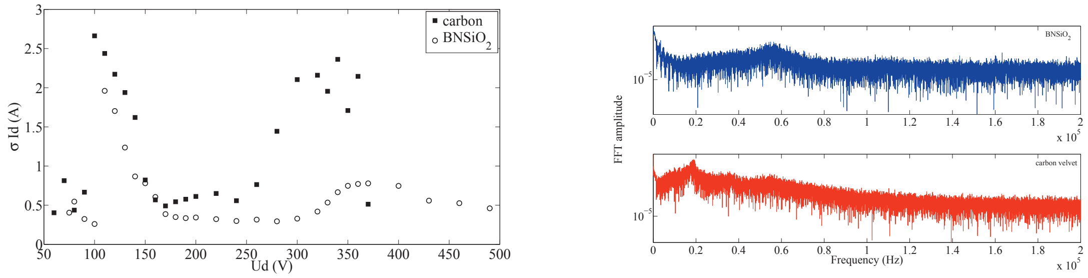

(a) (b)

Figure 3. (a) Discharge current standard deviation versus voltage for $BNSiO_2$ and carbon velvet, (b) frequency content of discharge current signals for $BNSiO_2$ (top) and carbon velvet (bottom) at 300 V

with velvet, whereas we observe higher currents with velvet than for $BNSiO_2$.

We believe that the very different operating characteristics of the thrusters used account for these differences. As shown in more recent measurements,[12] the 2kW thruster used by Raitses and colleagues shows somewhat atypical behavior. As the voltage is increased from 350 to 700 V, the peak electric field (deduced from emissive probe measurements) shifts a distance of 15 mm from the interior to the exterior of the thruster with BN walls. In contrast, the use of carbon velvet inserts localizes the electric field peak at these voltages to the vicinity of the exit plane in this thruster. Carbon velvet appears to shift their thruster to conventional, optimized operation. In our case, carbon velvet has an entirely different effect when used in a thruster which already operates optimally (Fig. 4(a)).

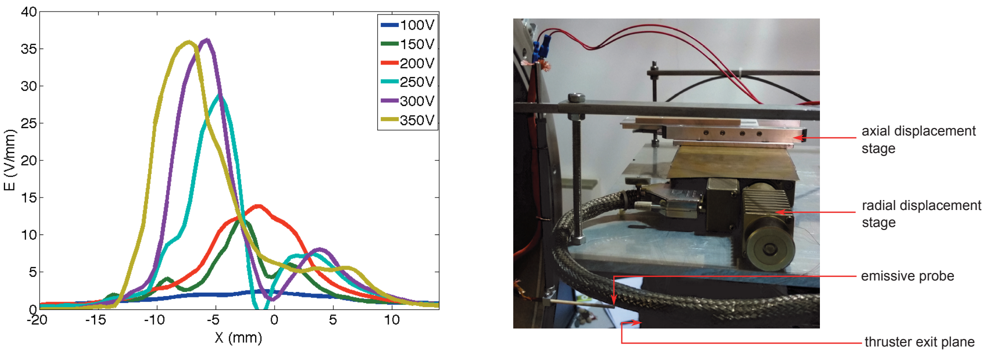

(a) (b)

Figure 4. (a) Electric field profiles determined by emissive probe, as a function of voltage, for carbon velvet, (b) photo of emissive probe mounting

Fig. 4(a) shows the electric field profiles obtained using an emissive probe with carbon velvet walls. For a similar thruster, operating with $BNSiO_2$ walls and under the same conditions, we note that the electric field maximum remains with 5 mm of the exit plane over a voltage range of 300 - 700 V.[10] In contrast, with carbon velvet, we observe the electric field maximum retreating into the channel as voltage increases from 200 to 350 V. At 350 V, the shift of the field maximum so far into the channel means that the particle acceleration can occur within the emissive ($BNSiO_2$) part of the channel. Additionally, the separation of the electric field from the magnetic field at higher voltages results in a progressive weakening of the electron confinement. This factor alone may account for the increase in electron current seen with the carbon velvet in our case, even without a consideration of an additional contribution to the electron current from turbulence.

The use of the carbon velvet inserts produces a clear effect on the accelerating electric field profile. On the one hand, as in Raitses' work, the inserts can produce dramatically improved performance for a non-optimal thruster. On the other, the inserts can degrade both the accelerating profile and electron confinement in an optimized thruster, leading to paradoxically higher currents even when electron emission is partially suppressed. The changes to thruster behavior have a marked effect on the features of the electron cyclotron instability as well; some of these changes are discussed in the next section.

IV. Role of the electron cyclotron drift instability with non-emissive and emissive walls

Radial-azimuthal simulations reveal the degree to which the electron cyclotron drift instability influences plasma-wall interaction, and ultimately, its influence on the anomalous electron current. We summarize here some key effects it creates; simulation results are outlined in-depth in 2013 paper of Héron and Adam.

(i) The electron cyclotron mode possesses radial, azimuthal and axial components, as found in experiments and simulations, and produces particle heating in all three directions. It causes complex modulation of the sheath potential, spatially (in the azimuthal direction) and temporally. The increase in the sheath potential results in increased SEE.
(ii) The mode produces a spread in energy of the emitted electrons transiting between the walls. These cold beams of emitted electrons have been observed in 1D simulations by Sydorenko and colleagues.[13] However, the action of the mode and the effect of channel curvature in 2D reveal additional effects: diffusion of the electron beams and the asymmetry of the wall emission.
(iii) The interaction between the mode and the cold emitted electron beams can result in a transition to a "beam-plasma" regime, which is associated with a sharp increase in the electron current, and possibly, the appearance of highly-unstable operating regimes.

To illustrate the link between the instability and current, we show the PIC simulation result[5] comparing the evolution of the current with the work produced by the instability in Fig. 5(a).

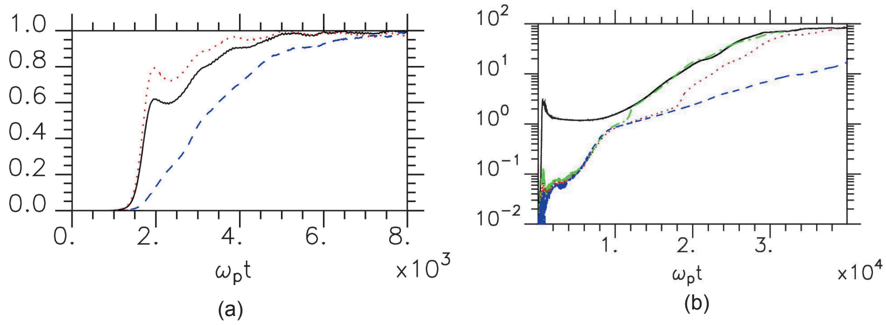

Figure 5. (a) axial current density (black line), azimuthal electric field work on particles (red dotted line) and radial electric field work on particles (blue dashed line). All quantities have been normalized. (b) PIC radial-azimuthal simulation result[5] for the evolution of the axial current as a function of time ($\omega_p t$ of 8000 = 0.24 μs) for materials of different emissivities. In black: $\epsilon^* = 20$ eV; in green: $\epsilon^* = 30$ eV; in red: $\epsilon^* = 50$ eV; in blue: $\epsilon^* = 1000$ eV

In Fig. 5(a), three normalized quantities are plotted with time ($\omega_p t$ of 8000 corresponds to 0.24 μs, for an ω_p of 3×10^{10} rad/s in the simulations). These quantities are the axial current density, the work produced by the azimuthal electric field on the electrons (in the reference frame of the electrons), and the work produced by the radial field on the electrons. All the quantities evolve in the same manner; the increase in anomalous current occurs on the same time scale as the heating produced by the instability.

Further interesting observations concerning the current evolution may be made when materials of different emissivities are considered (Fig. 5(b)). In this figure, at the start of the simulation, the high current regime is immediately attained with a material of low crossover energy ($\epsilon^* = 20$ eV, black line) and high emissivity. However, for lower emissivities, ($\epsilon^* = 30$ (green), 50 (red) and 1000 eV (blue)) the currents are lower and identical up to $\omega_p t$ of 8000. Up to this point, the current is dominated by the "direct" contribution from the electron cyclotron instability. At later times, progressive jumps in current are seen for the 30 and 50 eV materials, associated with the emergence of the beam-plasma instability.

In our experimental study, carbon velvet would correspond to the zero emission material ($\epsilon^* = 1000$ eV) for which lower currents would be expected, according to Fig. 5(b), due to the absence of emitted electrons (and the absence of the beam-plasma instability). Yet in reality, we observe higher currents in carbon velvet than in $BNSiO_2$. As discussed earlier, this is very likely to be due to the changes to the maximum electric field location encountered with the carbon velvet. Such changes are not taken into account in the radial-azimuthal simulations, where the electric field is imposed.

In the collective scattering experiments, the intensity of the density fluctuations associated with the instability is quantified via the form factor. The dynamic form factor $S(k, \omega)$ expresses the intensity of such fluctuations at a particular wavenumber k over a range of frequencies ω, and is obtained from the signal spectrum (normalized to remove noise contributions) and experiment parameters such as laser power and detector efficiency.[14] The dynamic form factor is integrated over the frequency range in which the signal of interest is present to give the absolute (unitless) static form factor $S(k)$.

A comparison of the form factors for the two materials provides an idea of the magnitude of the turbulent fluctuations associated with the mode. In the following, the wavenumber is set to an arbitrary value of 5780 rad/m; plasma conditions are a discharge voltage of 150 V and a flow rate of 3.5 mg/s.

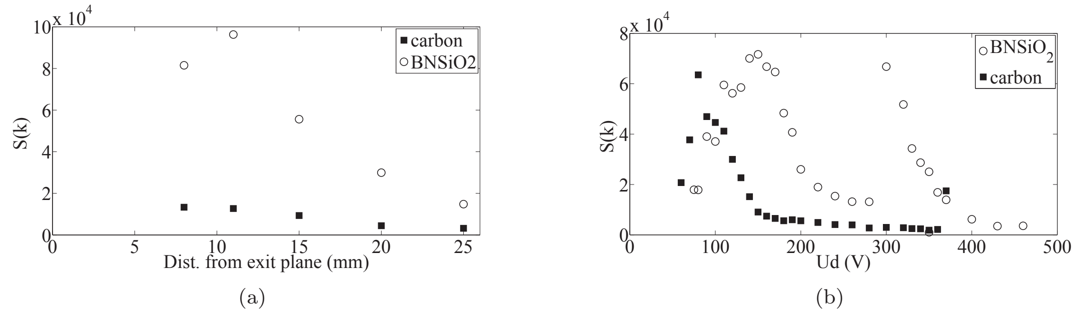

Figure 6. (a) Evolution in electron cyclotron mode amplitudes with axial distance from the thruster exit plane for $BNSiO_2$ and carbon velvet, (b) evolution in electron cyclotron mode amplitudes with voltage for $BNSiO_2$ and carbon velvet

In Fig. 6(a), the mode amplitudes for $BNSiO_2$ increase after the thruster exit plane to a maximum at about 1 cm, consistent with measurements we have made in the past. In contrast, for carbon velvet no such maximum in amplitude is seen and the mode amplitudes are much lower. With the retreat of the electric field further into the channel seen with carbon velvet, the location of the maximum E/B value also retreats into the channel. The mode growth rate increases with the drift velocity, and the highest mode amplitudes are likely to be seen inside the channel with velvet. Our measurements, which are restricted to the plasma region outside the exit plane due to the requirement of a free path for the laser beams, would miss any signal peak inside the channel, should it exist.

In Fig. 6(b), the variation of the mode amplitudes as a function of voltage for the two materials shows clear differences. In this figure, note that all measurements are performed at 11 mm from the exit plane and for a flow rate of 3.5 mg/s as the discharge voltage is varied. After 100 V, the mode amplitude with $BNSiO_2$ is consistently higher than for carbon velvet, but as discussed above, the movement of the electric field into the channel as voltage increases could hide the maximum mode amplitudes encountered with carbon velvet. At voltages below 100 V, however, the carbon velvet amplitude mode amplitude exceeds that observed with $BNSiO_2$. In the absence of wall emission in carbon velvet, the discharge would rely on other mechanisms, such as the electron cyclotron instability, to furnish the necessary electron current.

V. Conclusions

The nature of plasma-wall interaction in the Hall thruster is complicated not only by the presence of instabilities and secondary electron emission, but by their non-linear interaction. Our recent measurements indicate that the use of non-emitting inserts at the thruster exit plane, as a means of controlling wall emission, results in a cascade of effects which alter thruster operation. The electric field profile is shifted upstream, with consequences not only for particle acceleration and plasma interaction with the walls, but also for the small-scale electron density fluctuations.

In radial-azimuthal PIC simulations, the small-scale electron cyclotron drift instability contributes to electron current by its direct interaction with the electrons (demonstrated previously in axial-azimuthal simulations) and by its coupling to the wall emission. The instability enhances wall emission by heating the plasma radially, causes spatial and temporal fluctuations in the sheath potential, and provokes a transition to a high-current, beam-plasma regime.

In the current collective scattering studies of the mode, we are limited to observation of fluctuations outside the thruster channel, and the shifting of the electric field upstream makes some fluctuation measurements inaccessible with carbon velvet. In 2D radial-azimuthal simulations, the dynamic nature of the axial electric field is not represented. Nevertheless, these insights from scattering experiments and simulations reveal the extent to which changing the wall material influences the discharge and microturbulence features. Future work will examine intermediate materials such as alumina, and discharge current and cyclotron mode correlations.

Acknowledgments

The authors thank the GIS PPE (*Propulsion par Plasma dans l'Espace*) for funding of this work. S. T. thanks Dr. Y. Raitses for very helpful discussions regarding the use of carbon velvet electrodes.

References

[1]D. W. Forslund, R. L. Morse, and C. W. Nielson. Electron Cyclotron Drift Instability. Phys. Rev. Lett. **25**, 1266 (1970)

[2]S. P. Gary and J. J. Sanderson. Longitudinal waves in a perpendicular collisionless plasma shock. I. Cold ions. J. Plasma Phys. **4**, 739 (1970)

[3]J-C. Adam, A. Héron and G. Laval. Study of stationary plasma thrusters using two-dimensional fully kinetic simulations. Phys. Plasmas **11**, No. 1, pp. 295-305 (2004)

[4]S. Tsikata, N. Lemoine, V. Pisarev and D. Grésillon. Dispersion relations of electron density fluctuations in a Hall thruster plasma, observed by collective light scattering. Phys. Plasmas **16**, 033506 (2009)

[5]A. Héron and J-C. Adam. Anomalous conductivity in Hall thrusters: effects of the non-linear coupling of the electron-cyclotron drift instability with secondary electron emission of the walls. Phys. Plasmas **20**, 082313 (2013)

[6]S. Tsikata. *Small-scale electron density fluctuations in the Hall thruster, investigated by collective light scattering.* PhD thesis, Ecole Polytechnique (2009)

[7]Y. Raitses, D. Staack, A. Dunaevsky, and N. J. Fisch. Operation of a segmented Hall thruster with low-sputtering carbon-velvet electrodes. J. Appl. Phys. **99**, 036103 (2006)

[8]Y. Raitses, A. Smirnov, D. Staack, and N. J. Fisch. Measurements of secondary electron emission effects in the Hall thruster discharge. Phys. Plasmas **13**, 014502 (2006)

[9]S. Mazouffre, A. Pétin, P. Kudrna and M. Tichỳ. *Development of a high-frequency emissive probe system for plasma potential measurements in a Hall thruster.* IEEE Trans. Plasma Sci. **43**, 29 (2015)

[10]D. Gawron. *Phénomènes de transport ionique dans le plasma d'un propulseur à effet Hall à forte puissance: étude par spectroscopie laser.* PhD thesis, Université d'Orléans (2007)

[11]S. Barral, K. Makowski, Z. Peradzyński, N. Gascon, and M. Dudeck. Wall material effects in stationary plasma thrusters. II. Near-wall and in-wall conductivity. Phys. Plasmas **10**, 4137 (2003)

[12]Y. Raitses, I. D. Kaganovich, A. Khrabrov, D. Sydorenko, N. J. Fisch, and A. Smolyakov. *Effect of Secondary electron emission on electron cross-Field Current in E x B discharges.* IEEE Trans. Plasma Sci. **39**, 995 (2011)

[13]D. Sydorenko, A. Smolyakov, I. Kaganovich and Y. Raitses. Kinetic simulation of secondary electron emission effects in Hall thrusters. Phys. Plasmas **13**, 014501 (2006)

[14]D. Grésillon, C. Stern, A. Hémon, A. Truc, T. Lehner, J. Olivain, A. Quéméneur, F. Gervais, and Y. Lapierre, Phys. Scr. **T2B**, 459 (1982)